Journal of Thermal Analysis and Calorimetry (2019) 135:3485–3497
https://doi.org/10.1007/s10973-018-7520-4

Numerical analysis of natural convection of Cu–water nanofluid filling triangular cavity with semicircular bottom wall

A. S. Dogonchi[1] · Muneer A. Ismael[2] · Ali J. Chamkha[3,4] · D. D. Ganji[5]

Received: 2 May 2018 / Accepted: 30 June 2018 / Published online: 10 July 2018

Abstract

This study provides numerical analysis of the free convection of copper–water-based nanofluid filling a triangular cavity with semicircular bottom wall. The cavity sidewalls are maintained at cold temperature, while the semicircular wall is maintained at hot temperature. The other wall segments are thermally insulated. To control the energy transport within the cavity, a uniform magnetic field is applied horizontally. The physical domain is discretized according to the control volume finite element method which has been used to solve the governing equations. The physical and geometrical aspects of the current problem are investigated by inspecting the impacts of Rayleigh number, Hartman number, aspect ratio and the volume fraction of the Cu nanoparticles. Decreasing the radius of the hot semicircle enlarges the average Nusselt number at the absence of the magnetic field. When the magnetic field is applied, this effect is conversed within $Ra \leq 10^4$. This conversed impact does not hold up when Ra is raised to 10^5. The numerical results are correlated in a sophisticated correlation of the average Nusselt number with other parameters.

Keywords Nanofluid · Natural convection · Magnetic field · CVFEM · Nusselt number

List of symbols

Ha	Hartmann number (–)
Pr	Prandtl number (–)
B_0	Magnetic field (–)
c	Specific heat (J kg^{-1} K^{-1})
T	Temperature (K)
$Nu_{\text{loc.}}$	Local Nusselt number (–)
$Nu_{\text{ave.}}$	Average Nusselt number (–)
k	Thermal conductivity (W m^{-1} K^{-1})
u, v	Velocity components in x and y directions, respectively (m s^{-1})
Ra	Rayleigh number (–)
AR	Aspect ratio (–)
p	Pressure term (Pa)

Greek symbols

β	Thermal expansion coefficient (K^{-1})
ρ	Density (kg m^{-3})
μ	Dynamic viscosity (kg m^{-1} s^{-1})
ν	Kinematic viscosity (m^2 s^{-1})
σ	Electrical conductivity (Ω^{-1} m^{-1})
ϕ	Nanoparticles volume fraction (–)
θ	Dimensionless temperature

Subscripts

f	Base fluid
nf	Nanofluid
s	Solid nanoparticles

✉ A. S. Dogonchi
Sattar.dogonchi@yahoo.com

✉ Muneer A. Ismael
muneerismael@yahoo.com

✉ Ali J. Chamkha
achamkha@pmu.edu.sa

[1] Young Researchers and Elite Club, Aliabad Katoul Branch, Islamic Azad University, Aliabad Katoul, Iran

[2] Mechanical Engineering Department, University of Basrah, Basra, Iraq

[3] Mechanical Engineering Department, Prince Sultan Endowment for Energy and Environment, Prince Mohammad Bin Fahd University, Al-Khobar 31952, Saudi Arabia

[4] RAK Research and Innovation Center, American University of Ras Al Khaimah, Ras al-Khaimah, United Arab Emirates

[5] Mechanical Engineering Department, Babol Noshirvani University of Technology, Babol, Iran

Introduction

In recent years, researchers have used many methods to increase the heat transfer coefficient. One of them is to add metallic nanoscale particles to the base fluids. This combination, which is called 'nanofluid,' has higher thermal conductivity than normal fluids. Many studies have been done on the flow and heat transfer of the nanofluids [1–21]. The mixed convection of Cu–water nanofluid in lid-driven trapezoidal cavities under the magnetic field effect was analyzed by Chamkha and Ismael [1]. Nanofluid natural convection flow and heat transfer in a circular-wavy cavity were studied by Hatami et al. [2]. Magneto-hydrodynamic (MHD) nanofluid toward a stagnation point flow over a permeable stretching surface was studied by Bhatti and Rashidi [3]. They detected that the velocity of the fluid grows due to greater impact of magnetic field and porosity parameter. The buoyancy-driven heat transfer increment in a sinusoidal heated enclosure applying hybrid nanofluid was studied by Tayebi and Chamkha [4]. Dogonchi and Ganji [5] examined the unsteady squeezing magneto-hydrodynamic flow and heat transfer of nanofluid between two parallel plates under the impacts of thermal radiation and Cattaneo–Christov heat flux model. Nanofluid flow and heat transfer between non-parallel plates under the magnetic field were analyzed by Dogonchi and Ganji [6]. Mixed convection of Al_2O_3–water nanofluid over permeable wedge considering aggregation effects was studied by Ellahi et al. [7]. Squeezing unsteady nanofluid flow between two parallel plates was explored by Dib et al. [8]. Hayat et al. [9] investigated the nanofluid flow through a porous space with convective conditions and heterogeneous–homogeneous reactions. Hayat et al. [10] studied the impacts of homogeneous–heterogeneous reactions on the nanofluid flow. Rashidi et al. [11] explored the impact of the thermal radiation on the magneto-hydrodynamic buoyancy flow of nanofluid over a stretching sheet. Williamson nanofluid flow over a porous shrinking/stretching sheet under the thermo-diffusion and thermal radiation impacts was discussed by Bhatti and Rashidi [12].

Despite its active enhancement of heat transfer, the mixed convection is fulfilled by nanofluids as extra strategy to enhance heat transfer in enclosures. With the aid of nanofluids, variant enclosure geometries, inner rotating bodies, impinging jet mechanism, moving wall mechanisms have been studied by [22–27].

Researchers have also focused on the natural convection of nanofluids and normal fluids in the enclosures [28–42]. Natural convection of nanofluid and entropy generation in a cavity with variable temperature side walls were investigated by Sheremet et al. [28]. They applied Buongiorno's mathematical model in their work. Ghalambaz et al. [29] examined the phase-change heat transfer of nanofluid in a

Table 1 Thermo-physical properties of water and nanoparticles

	ρ/kg m^{-3}	C_p/J kg^{-1} K^{-1}	k/W mK^{-1}
Copper (Cu)	8933	385	401
Pure water	997.1	4179	0.613

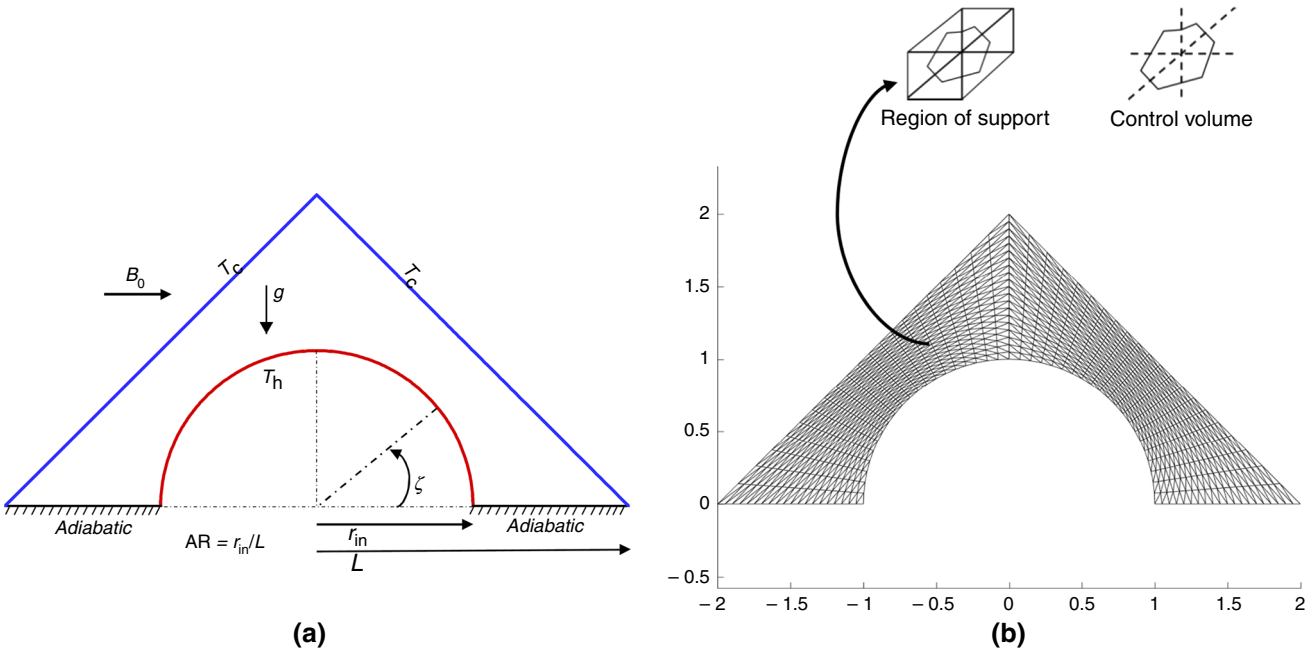

Fig. 1 **a** Physical model and coordinate system **b** grid distribution

cavity heated from below. Alsabery et al. [30] perused the conjugate natural convection of nanofluid in a cavity considering sinusoidal temperature variations on both horizontal sides. The impact of magnetic field and internal heat generation on the free convection flow of nanofluid in a rectangular cavity was studied by Rashad et al. [31]. Their results indicate that the average Nusselt number diminishes as the Hartmann number or the solid volume fraction raises, while the opposite treatment happens with the raise in magnetic field inclination angle. Natural convection of nanofluid inside a porous wavy cavity considering the impact of thermal dispersion was examined by Sheremet et al. [32]. They demonstrated that the heat transfer rises with Rayleigh number, dispersion parameter and undulation number, while convective flow is abated with a rise in undulation number, flow inertia parameter and dispersion parameter. Natural convection of nanofluid in a portion cavity was studied by Bararnia et al. [33]. They applied the lattice Boltzmann method to solve governing equations. Abu-Nada et al. [34] investigated the convective heat transfer increment in horizontal concentric annuli applying nanofluids. Jou and Tzeng [35] did numerical research of natural convective heat transfer increment in rectangular enclosures filled with nanofluids. Dogonchi et al. [36] explored the nanofluid natural convective heat transfer in a wavy enclosure. They stated that for higher Rayleigh number there is an optimum volume fraction of nanofluid in which the average Nusselt number is maximum. Selimefendigil et al. [37] investigated the generation of entropy in entrapped trapezoidal enclosures filled with nanofluid under the influence of magnetic field. Sheremet et al. [38] studied the free convection of nanofluid in a partially heated wavy porous cavity considering the impacts of Brownian diffusion and thermophoresis. Recently, Selimefendigil and Oztop [43] have developed a mathematical model based on proper orthogonal decomposition and polynomial interpolation among modal coefficients to study the 3D natural convection of CuO–water nanofluid-filled trapezoidal cavity with corrugated wall.

This paper studies Cu–water nanofluid natural convection flow and heat transfer in a triangular enclosure of semicircular bottom wall under the magnetic field impact employing the Control Volume Finite Element Method (CVFEM). Cooling of circular hot surfaces using a high-thermal-conductivity medium like nanofluid is of major importance in industrial applications. The circular surface can simulate a heat exchanger pipe or solidification of melting metal. The existence of the magnetic field is to control these physical problems. The impacts of effective parameters such as Rayleigh number, volume fraction of nanofluid, Hartmann number and aspect ratio on flow and heat transfer characteristics are explored and demonstrated graphically.

Problem description

Cu–water nanofluid natural convection flow in an enclosure under the magnetic field is investigated. Physical model and sample grid distribution of the present paper are shown in Fig. 1. The inner circular wall is maintained at a constant temperature T_h, while the outer inclined walls are maintained at a constant temperature T_c such that $T_h > T_c$. In addition, the horizontal walls are adiabatic. Under the Boussinesq approximation, the continuity, momentum and energy equations for steady two-dimensional Cu–water nanofluid natural convection flow in the enclosure can be stated as:

$$\frac{\partial u}{\partial x}+\frac{\partial v}{\partial y}=0 \tag{1}$$

$$u\frac{\partial u}{\partial x}+v\frac{\partial u}{\partial y}=-\frac{1}{\rho_{nf}}\frac{\partial p}{\partial x}+\frac{\mu_{nf}}{\rho_{nf}}\left(\frac{\partial^2 u}{\partial x^2}+\frac{\partial^2 u}{\partial y^2}\right) \tag{2}$$

$$u\frac{\partial v}{\partial x}+v\frac{\partial v}{\partial y}=-\frac{1}{\rho_{nf}}\frac{\partial p}{\partial y}+\frac{\mu_{nf}}{\rho_{nf}}\left(\frac{\partial^2 v}{\partial x^2}+\frac{\partial^2 v}{\partial y^2}\right)+\beta_{nf}g(T-T_c)-\frac{\sigma_f B_0^2}{\rho_{nf}}v \tag{3}$$

Table 3 Impact of grid size on the average Nusselt number (Nu_{ave}) when $Ra = 10^5$, $\phi = 0.04$, $Ha = 50$ and AR = 0.5

Grid dimension (radial direction × angular direction)	Nu_{ave}
31 × 101	4.041443
41 × 131	4.068598
51 × 161	4.076842
61 × 191	4.078895
71 × 221	4.078636
81 × 251	4.077489

Table 2 Comparison between present results and other works for the average Nusselt number (Nu_{ave})

Ra	Present work	Khanafer et al. [45]	%Error	De Vahl Davis [46]	%Error
10^3	1.1307	1.118	1.136	1.118	1.136
10^4	2.2674	2.245	0.998	2.243	1.087
10^5	4.5851	4.522	1.395	4.519	1.463
10^6	8.8341	8.826	0.0918	8.799	0.399

$$u\frac{\partial T}{\partial x}+v\frac{\partial T}{\partial y}=\frac{k_{\mathrm{nf}}}{(\rho C_{\mathrm{p}})_{\mathrm{nf}}}\left(\frac{\partial^2 T}{\partial x^2}+\frac{\partial^2 T}{\partial y^2}\right) \tag{4}$$

Here u and v are the velocities in the x and y directions, respectively, T is the temperature, P is the pressure, σ_{f} is the electric conductivity of the fluid, and B_0 is the magnetic field. Further, ρ_{nf} is the nanofluid effective density, $(\rho Cp)_{\mathrm{nf}}$ is the nanofluid heat capacitance, β_{nf} is the nanofluid thermal expansion coefficient, μ_{nf} is the nanofluid effective dynamic viscosity, and k_{nf} is the thermal conductivity of nanofluid which are defined as follows:

$$\rho_{\mathrm{nf}}=(1-\phi)\rho_{\mathrm{f}}+\phi\rho_{\mathrm{s}} \tag{5}$$

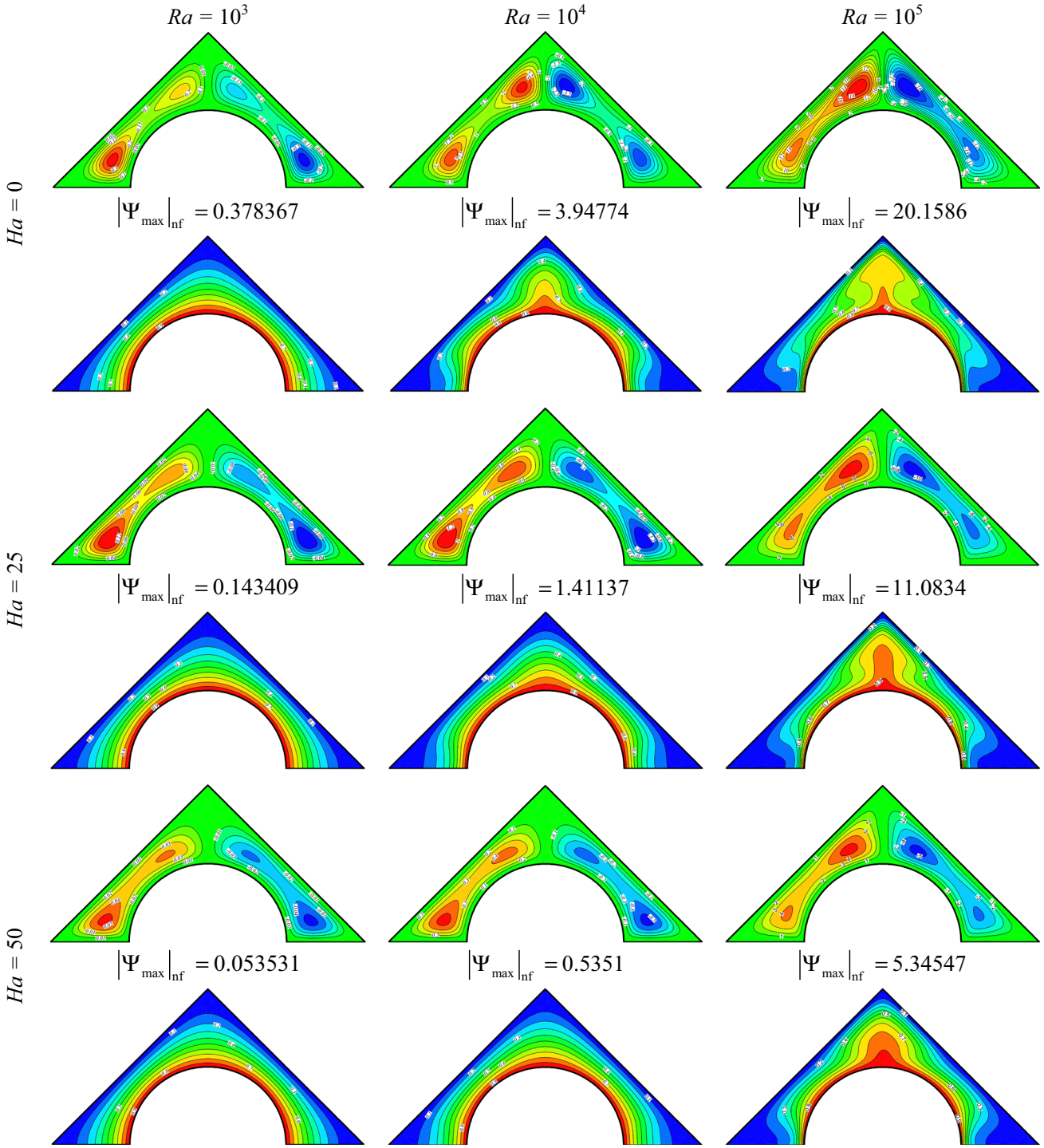

Fig. 2 Streamlines and isotherms for different values of *Ra* and *Ha* when $\phi = 2\%$ and AR = 0.5

$$(\rho C_p)_{nf} = (1-\phi)(\rho C_p)_f + \phi(\rho C_p)_s \tag{6}$$

$$(\beta)_{nf} = (1-\phi)\beta_f + \phi\beta_s \tag{7}$$

$$\mu_{nf} = \frac{\mu_f}{(1-\phi)^{2.5}} \tag{8}$$

$$\frac{k_{nf}}{k_f} = \frac{k_s + 2k_f - 2\phi(k_f - k_s)}{k_s + 2k_f + 2\phi(k_f - k_s)}. \tag{9}$$

The nanofluid thermo-physical properties are stated in Table 1.

The stream function and vorticity are defined as follows:

$$u = \frac{\partial \psi}{\partial y}, \quad v = -\frac{\partial \psi}{\partial x}, \quad \omega = \frac{\partial v}{\partial x} - \frac{\partial u}{\partial y} \tag{10}$$

We define these dimensionless variables as:

$$X = \frac{x}{L}, \quad Y = \frac{y}{L}, \quad \Omega = \frac{\omega L^2}{\alpha_f}, \quad \Psi = \frac{\psi}{\alpha_f}, \quad U = \frac{uL}{\alpha_f}, \quad V = \frac{vL}{\alpha_f}, \quad \theta = \frac{T - T_c}{T_h - T_c} \tag{11}$$

By applying these dimensionless variables, the governing equations reduce to non-dimensional form:

$$\frac{\partial \Psi}{\partial Y}\frac{\partial \Omega}{\partial X} - \frac{\partial \Psi}{\partial X}\frac{\partial \Omega}{\partial Y} = \frac{\mu_{nf}}{\mu_f}\frac{\rho_f}{\rho_{nf}}\mathrm{Pr}\left(\frac{\partial^2 \Omega}{\partial X^2} + \frac{\partial^2 \Omega}{\partial Y^2}\right) + \frac{\beta_{nf}}{\beta_f}Ra\,\mathrm{Pr}\frac{\partial \theta}{\partial X} + \frac{\rho_f}{\rho_{nf}}Ha^2\,\mathrm{Pr}\frac{\partial^2 \Psi}{\partial X^2} \tag{12}$$

$$\frac{\partial \Psi}{\partial Y}\frac{\partial \theta}{\partial X} - \frac{\partial \Psi}{\partial X}\frac{\partial \theta}{\partial Y} = \frac{k_{nf}}{k_f}\frac{(\rho C_p)_f}{(\rho C_p)_{nf}}\left(\frac{\partial^2 \theta}{\partial X^2} + \frac{\partial^2 \theta}{\partial Y^2}\right) \tag{13}$$

$$\frac{\partial^2 \Psi}{\partial X^2} + \frac{\partial^2 \Psi}{\partial Y^2} = -\Omega \tag{14}$$

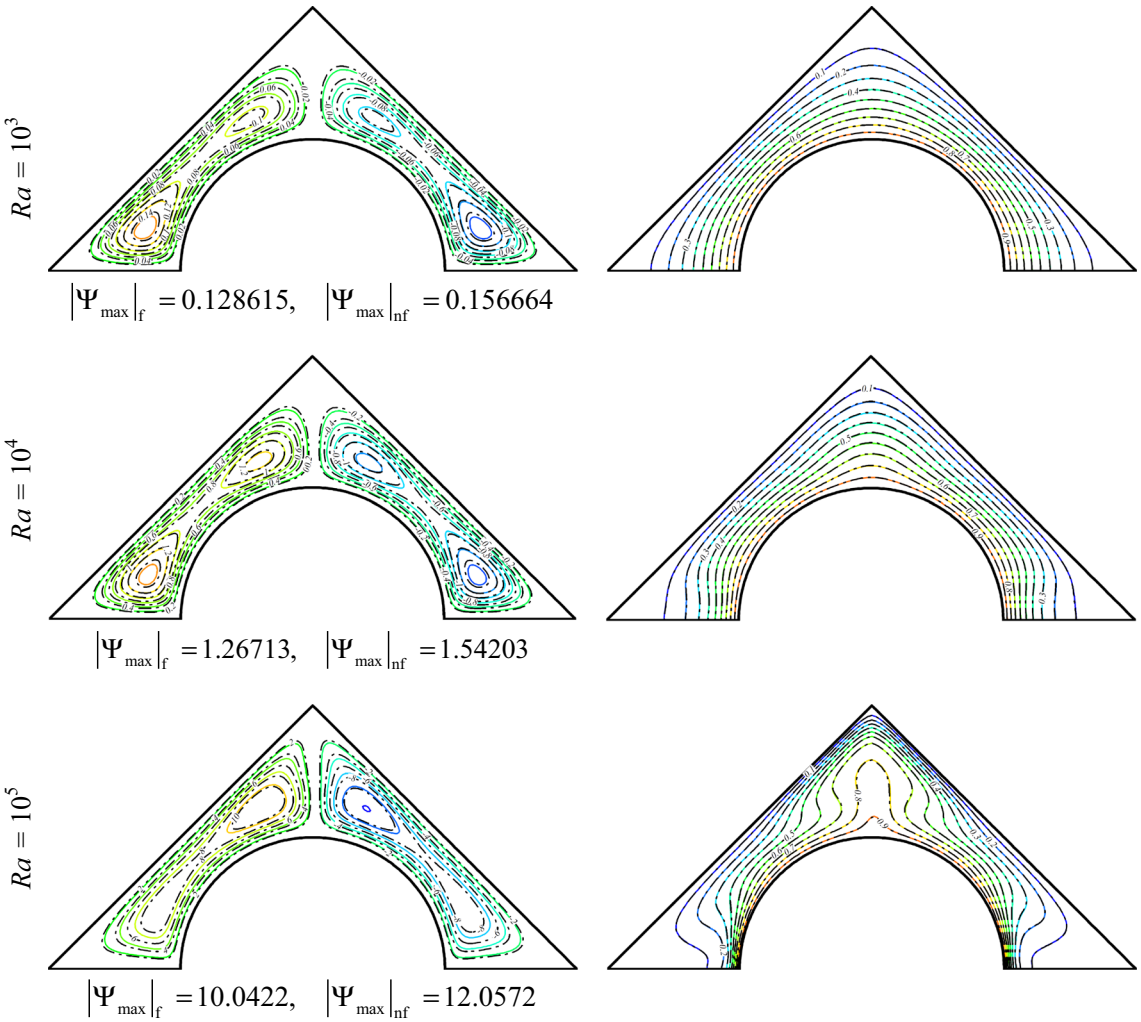

Fig. 3 Comparison of the streamlines and isotherms between nanofluid (dashed lines) and pure fluid (solid line) for different values of *Ra* when *Ha* = 25 and AR = 0.5

Subject to the boundary conditions:

$$\begin{aligned} &\theta = 1 && \text{on the inner circular wall}\\ &\theta = 0 && \text{on the outer inclined walls}\\ &\frac{\partial \theta}{\partial n} = 0 && \text{on the two other adiabatic walls}\\ &\Psi = 0 && \text{on the all walls} \end{aligned} \tag{15}$$

where $\mathrm{Pr} = \nu_f/\alpha_f$ is the Prandtl number, $Ra = g\beta_f(T_h - T_c)L^3/\alpha_f\nu_f$ is the Rayleigh number and $Ha = B_0 L\sqrt{\sigma_f/\mu_f}$ is the Hartmann number.

The Local and average Nusselt number along the hot circular wall can be stated as:

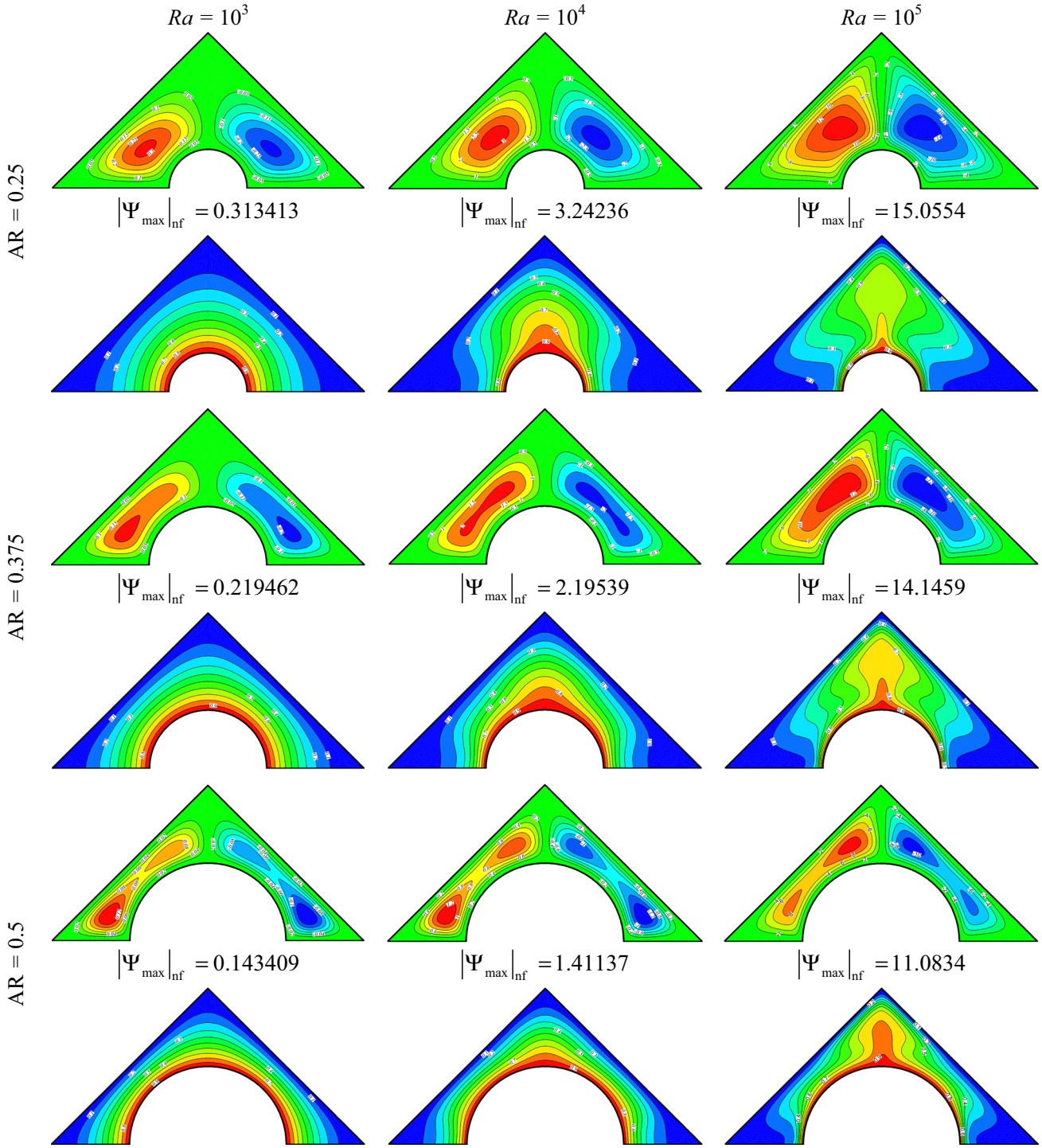

Fig. 4 Streamlines and isotherms for different values of *Ra* and AR when $\phi = 2\%$ and *Ha* = *25*

$$Nu_{\text{loc.}} = -\frac{k_{\text{nf}}}{k_{\text{f}}}\frac{\partial\theta}{\partial n} \tag{16}$$

$$Nu_{\text{ave.}} = \frac{1}{\pi}\int_0^{\pi} Nu_{\text{loc.}}\,\mathrm{d}\zeta \tag{17}$$

where n is the direction normal to the inner circular wall.

Numerical solution

The target of this part is to discuss the impacts of the effective parameters of this paper such as: Rayleigh number (Ra), volume fraction of nanofluid (ϕ), Hartmann number (Ha) and aspect ratio (AR), on the nanofluid natural convection in an enclosure. The governing equations are solved via Control Volume Finite Element Method (CVFEM) [44]. In accordance with the physical geometry mentioned above, we codified the CVFEM in a FORTRAN code and validated it by comparing its results with other studies stated in the literature [45, 46] (see Table 2). Table 2 delineates very good agreements between various results. It is worth mentioning that mesh-independent test has been carried out with respect to the average Nusselt number as shown in Table 3, which demonstrates that the grid of 61 × 191 should be chosen for this study.

Results and discussion

In this category, the numerical results obtained from varying the physical and geometrical parameters are displayed and discussed. Figure 2 portrays the alteration of the streamlines and isotherms with Rayleigh number (horizontally) and Hartman number (vertically) for aspect

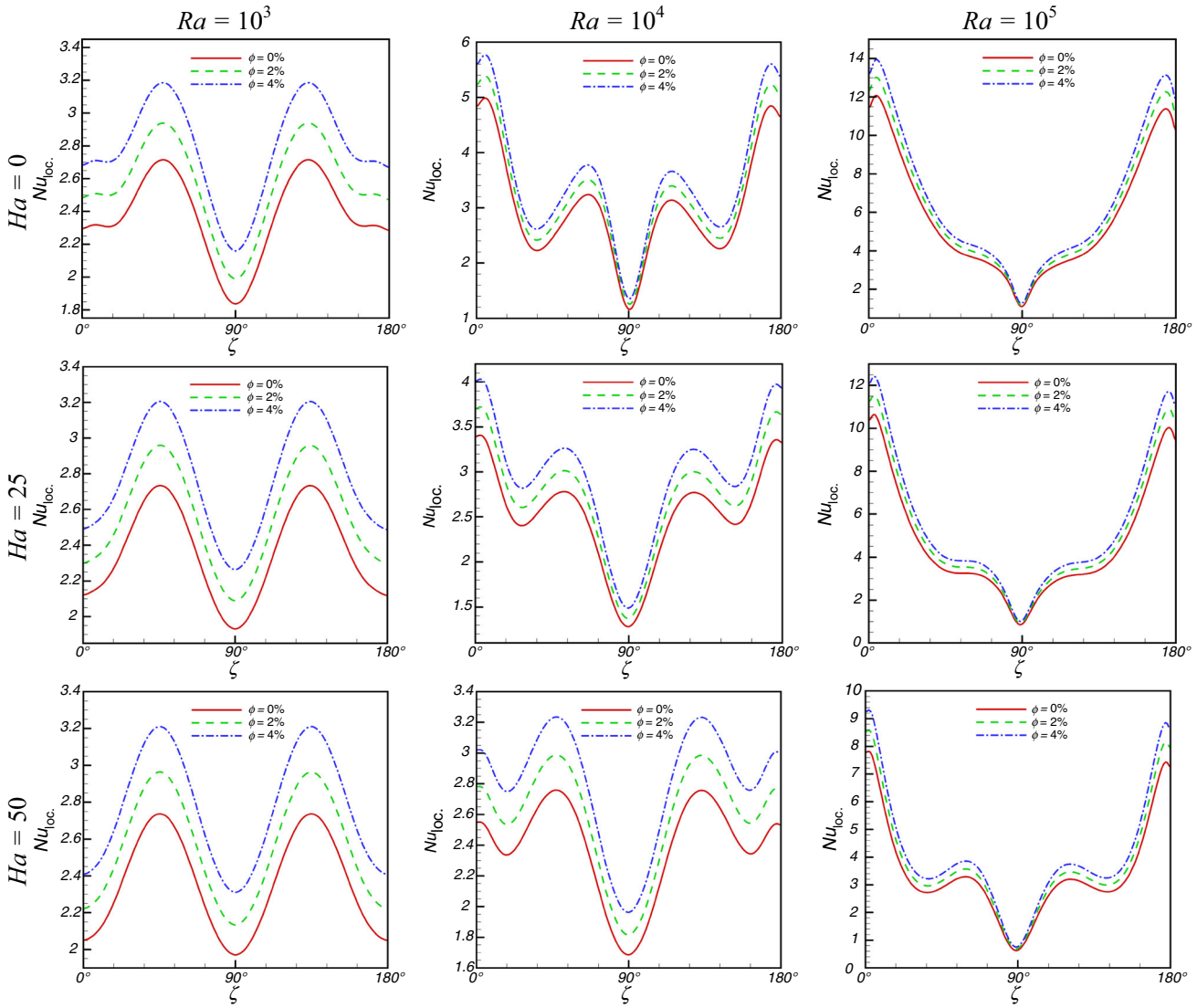

Fig. 5 Local Nusselt number ($Nu_{\text{loc.}}$) for different values of Ra, Ha and ϕ when AR = 0.5

ratio AR = 0.5 and volume fraction $\phi = 0.02$. The convective currents protrude from the semicircle wall toward the vertex of the cavity; thus, the streamlines form in two main counter rotating double-eyed vortices on both sides of the cavity. At $Ha = 0$, the magnetic drag force is absent; thus, the strength of the streamlines increases robustly and the isotherms pattern changes from uniform to plume-like behavior with increasing Ra. When the magnetic field is switched on and set at $Ha = 25$, the strengths of the streamlines decrease by 62, 64 and 45% at $Ra = 10^3$, 10^4 and 10^5, respectively, whereas they increase strongly with increasing Ra. The plume-like isotherms at this magnetic field are seen at $Ra = 10^5$ only. When the magnetic field is further increased such that $Ha = 50$, more reduction in streamlines strength compared with $Ha = 0$ is seen, which is characterized by 85.8, 86.4 and 73.5% reduction at $Ra = 10^3$, 10^4 and 10^5, respectively. The strength of the streamlines magnify by one order of magnitude with Ra, while the isotherms show less protruding front in such a way that even at $Ra = 10^5$, the plume behavior looks hesitant.

Figure 3 depicts comparison between streamlines and isotherms of pure fluid and nanofluid for different Ra numbers at AR = 0.5 and $Ha = 25$. These lines are mostly consistent, but the enhancement in the streamlines strength due to the addition of the nanoparticles ($\phi = 4\%$) is 21.8, 21.7 and 20% at $Ra = 10^3$, 10^4 and 10^5, respectively. These enhancements are accounted for the enhanced thermal conductivity, which boosts the convective currents. At $Ra = 10^5$, the convective currents are already strong, as

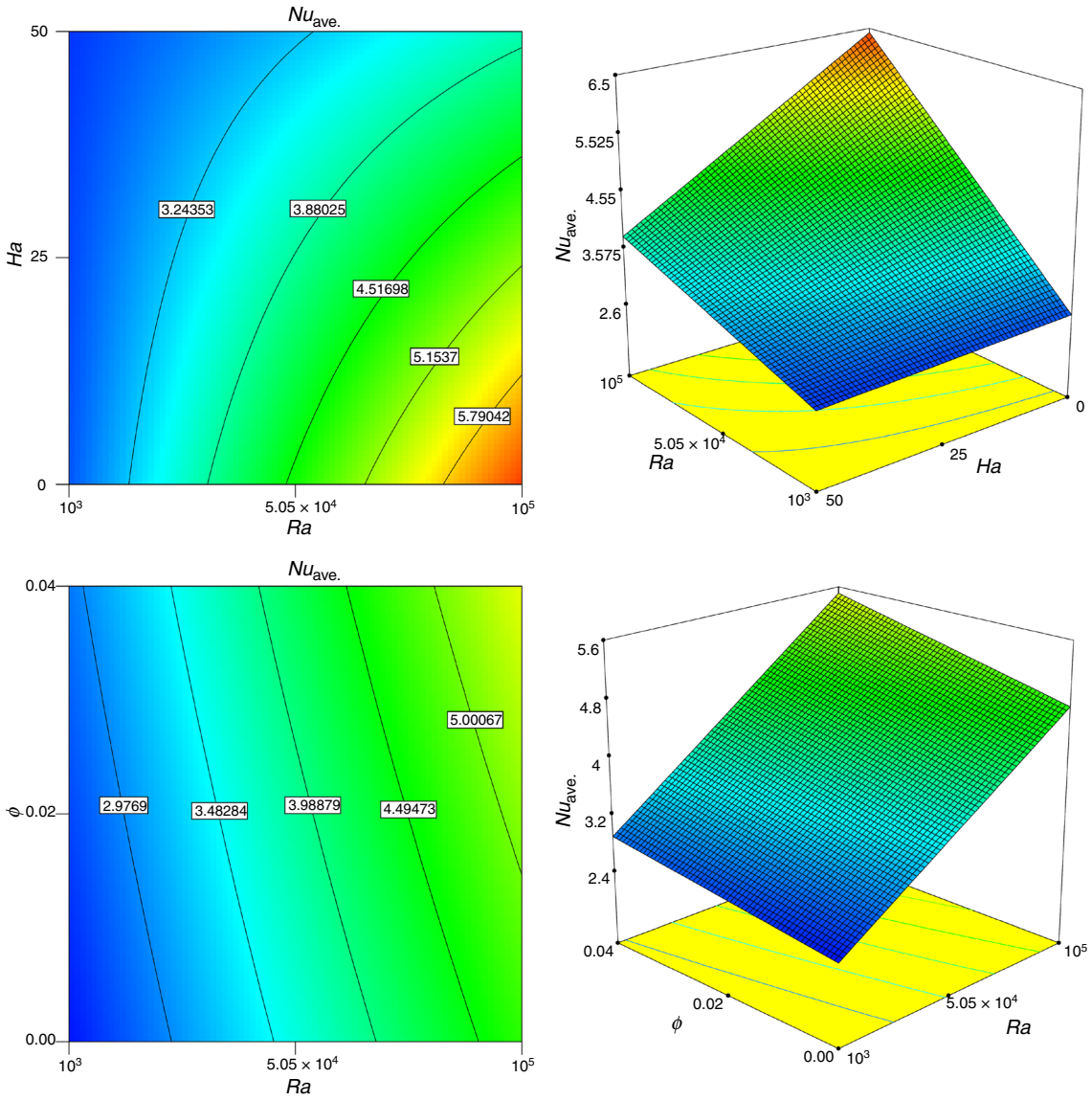

Fig. 6 Average Nusselt number ($Nu_{ave.}$) for different values of Ra, Ha and ϕ when AR = 0.5

such; the enhancement due to the nanoparticles addition is somewhat less than other lower values of *Ra*.

Figure 4 elucidates the effect of the space of cavity on the streamlines and the isotherms for different *Ra* number at *Ha* = 25 and ϕ = 0.02. The first row depicts the lowest aspect ratio (AR = 0.25), which corresponds to the larger feasible space; the nanofluid circulates freely and thus consists of single-eye attitude. When AR increases to 0.375, the feasible space is reduced; therefore, the recirculation shrinks and weakens in the form of 30, 32.3 and 6% according with *Ra* values of 10^3, 10^4 and 10^5, respectively. When AR is further increased to 0.5, the feasible space is more limited resulting in more shrink circulation with double-eye attitude, and extra weakening in the streamline strength reach to 54, 56 and 26% at corresponding to *Ra* values of 10^3, 10^4 and 10^5, respectively. It is worth noting that the reduction in the circulation strength with AR is less at $Ra = 10^5$; this is due to the dominance of the buoyancy force which is still effective despite the space limitation. The effect of aspect ratio can obviously be characterized by the appearance of thermal stratification which can be seen at the larger free space (AR = 0.25) at $Ra = 10^5$ due to the domination of the natural convection. At other aspect ratios, the plume-like appearance reveals the influence of the natural convection.

Figure 5 presents the local Nusselt number along the semicircle hot wall for different values of *Ra*, *Ha* and ϕ at AR = 0.5. At $Ra = 10^3$, the buoyancy force is relatively weak and the isotherms are almost uniform around the semicircle hot wall; therefore, we can see the "M"-shaped curves of Nusselt number manifest maximal values at

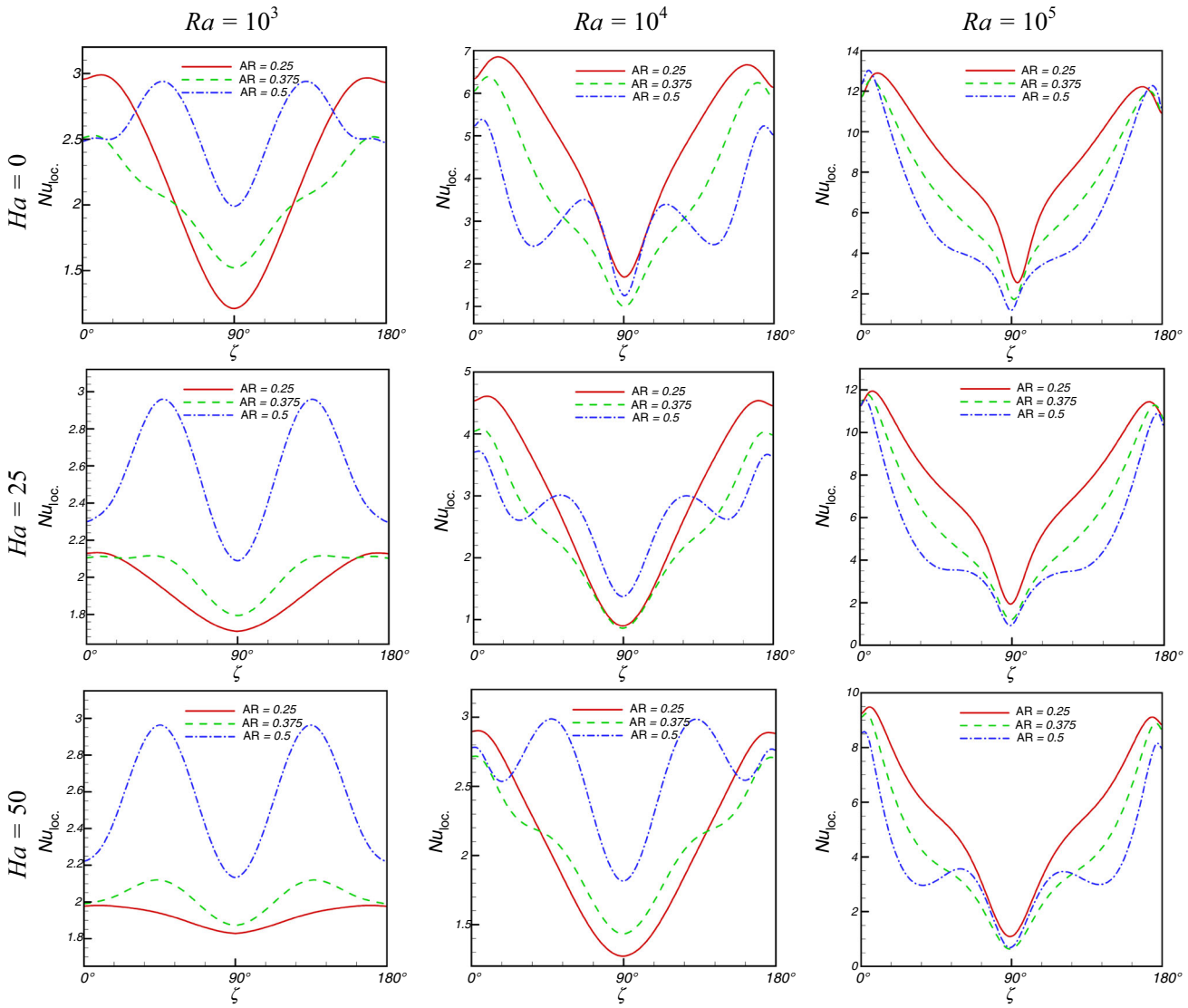

Fig. 7 Local Nusselt number ($Nu_{loc.}$) for different values of AR when $\phi = 2\%$

$\zeta = 45°$ and 135° where at these two locations, the distance to the cold walls is minimal. At $\zeta = 90°$, the distance to the vertex of the cavity is maximum; thus, minimum Nusselt number is recorded here. It is obvious that Hartman number has little impact at $Ra = 10^3$, because the buoyancy force is already weak. At $Ra = 10^4$, the buoyancy force is stronger; thus, the convective currents rise resulting in steeper thermal boundary layer along the hot surface except at $\zeta = 90°$, where the protruding isotherms thicken the thermal boundary layer, causing significant reduction in Nusselt number there. The effect of Ha is identified by lowering the Nusselt number along the hot surface. In addition, with increasing Ha, the Nusselt values look indolent and prominent at the edges of the surface and at $\zeta = 45°$, respectively. At $Ra = 10^5$, the fluctuations in Nusselt number disappear especially when $Ha \leq 25$. This is because the vigor buoyancy force forms the plume-like isotherm at $\zeta = 90°$, which means quite thick boundary layer causing the steep reduction in Nusselt number. Hartman number impedes the buoyancy force; thus, little fluctuation is seen when $Ha = 50$. However, the role of the nanoparticles is more pronounced at lower Ra values where they enhance the Nusselt number by enhancing the thermal conductivity. It is worth noting that at $\zeta = 90°$, the two

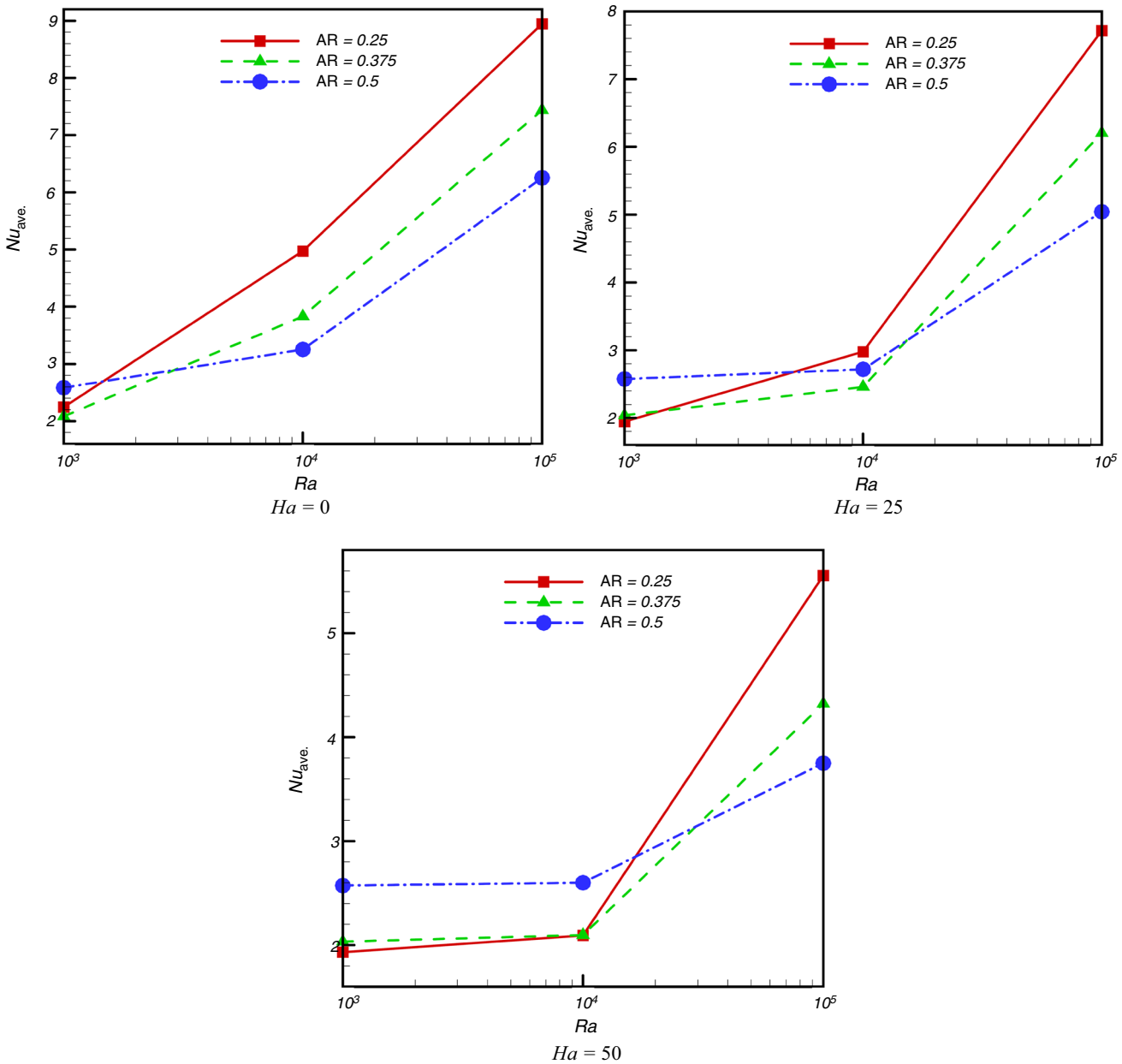

Fig. 8 Average Nusselt number ($Nu_{ave.}$) for different values of AR

circulations are met, and then, the nanofluid intensification is low; thus, increasing the volume of nanoparticles is ineffective.

Figure 6 depicts contour maps and surface presentation of the average Nusselt number for different ranges of Ra, Ha and ϕ at AR = 0.5. This figure elucidates that Nu_{ave} augments with Ra rapidly for zero magnetic field ($Ha = 0$), while it increases slowly with Ra for higher Ha numbers. This is due to the adverse effects of the buoyancy and Lorentz forces. On the other hand, the volume fraction of nanoparticles gives bit linear increase in Nu_{ave} compared with Ra number.

Figure 7 portrays the impact of the aspect ratio on the local Nusselt number along the hot surface for different Ra and Ha numbers at $\phi = 0.02$. The attribution of the local Nusselt number of AR = 0.5 is stated in Fig. 5. However, for lower AR values, the hot surface becomes farer from the cold sidewalls and more nanofluid fills the cavity, as such; the fluctuation of the local Nusselt number is notably reduced. The fluctuation decreases more and more with increasing Ha number. Nevertheless, the minimum local Nusselt number is still recorded at $\zeta = 90°$ owing to the reason stated above.

Although the decrease of AR means decreasing the segment of the source, which heats up the nanofluid, we see antithetical increase in the average Nusselt number. This behavior, as displayed in Fig. 8, refers to the feasible space that provides reinforced circulation resulting in transporting more energy. On the other hand, when the magnetic field is switched on, the feasible space occupies more fluid subjecting to the magnetic force; thus, adverse impact of decreasing aspect ratio is seen when $Ra \leq 10^4$. Nevertheless, this adverse impact does not hold up at higher Ra number where the buoyancy force is strong enough in such a way that the strong circulation resists the drag effect exerted by the magnetic field.

Most of the founded numerical data are utilized in establishing a comprehensive correlation relating the average Nusselt number with Ra, Ha and ϕ. The variation of Nusselt number with the aspect ratio AR manifests sophisticated behavior, and including AR in predicting the correlation can results in an unhandy correlation. Thus, we included only one value of the aspect ratio, that is AR = 0.5. The regression analysis has resulted in the following correlation;

$$\begin{aligned} Nu_{avg} &= 2.47844 + 3.51621 \times 10^{-5} \\ &\quad \times Ra - 1.20336 \times 10^{-3} \times Ha + 12.16801 \\ &\quad \times \phi - 5.02473 \times 10^{-7} \times Ra \times Ha \\ &\quad + 9.45666 \times 10^{-5} \times Ra \times \phi - 0.066757 \\ &\quad \times Ha \times \phi \end{aligned}$$

where $10^3 \leq Ra \leq 10^5$, $0 \leq Ha \leq 50$, $0.0 \leq \phi \leq 4\%$ and AR = 0.5.

It reveals the enhancing role of both Rayleigh number and the volume fraction of the nanoparticles and the depressing action of Hartman number. However, it has very good correlation factor, $R^2 = 0.9832$. This correlation facilitates the handy prediction of the average Nusselt number of the present geometry within the mentioned parameters ranges.

Conclusions

Natural convection in a triangular cavity with semicircle base filled with Cu–water nanofluid is studied numerically using control volume finite element method. The cavity is subjected to a constant transverse magnetic field, which generates a downward acting Lorentz force. The following observations are drawn from the results.

- When the magnetic field is amplified by raising Hartman number from 0 to 50, the strength of the streamlines drops by 85.8, 86.4 and 73.5% at $Ra = 10^3$, 10^4 and 10^5, respectively.
- Increasing the volume fraction of the copper nanoparticles from 0 to 0.04, the streamlines strengthen by 21.8, 21.7 and 20% at $Ra = 10^3$, 10^4 and 10^5, respectively, even in the presence of the magnetic field.
- Increasing the radius of the hot semicircle limits the space of nanofluid circulation and significantly weakens its strength. This attitude is less effective at high Rayleigh number.
- At the absence of the magnetic field, decreasing the radius of the hot semicircle enlarges the average Nusselt number. For nonzero magnetic field, this effect is conversed when $Ra \leq 10^4$. This conversed impact does not hold up when Ra is raised to 10^5.
- The controlled magnetic field provides good appliance by which the hot surfaces could be brought under effective operational performance.
- The established sophisticated correlation of the average Nusselt number contributes in determining the overall heat transfer with respect of Rayleigh number, Hartman number and the volume fraction of Cu nanoparticles.

References

1. Chamkha AJ, Ismael MA. Magnetic field effect on mixed convection in lid-driven trapezoidal cavities filled with a Cu–water nanofluid with an aiding or opposing side wall. J Therm Sci Eng Appl. 2016;8:031009–031009-12.

2. Hatami M, Song D, Jing D. Optimization of a circular-wavy cavity filled by nanofluid under the natural convection heat transfer condition. Int J Heat Mass Transf. 2016;98:758–67.
3. Bhatti MM, Rashidi MM. Numerical simulation of entropy generation on MHD nanofluid towards a stagnation point flow over a stretching surface. Int J Appl Comput Math. 2017;3:2275–89.
4. Tayebi T, Chamkha AJ. Buoyancy-driven heat transfer enhancement in a sinusoidally heated enclosure utilizing hybrid nanofluid. Comput Therm Sci. 2017;9:405–21.
5. Dogonchi AS, Ganji DD. Impact of Cattaneo–Christov heat flux on MHD nanofluid flow and heat transfer between parallel plates considering thermal radiation effect. J Taiwan Inst Chem Eng. 2017;80:52–63.
6. Dogonchi AS, Ganji DD. Analytical solution and heat transfer of two-phase nanofluid flow between non-parallel walls considering Joule heating effect. Powder Technol. 2017;318:390–400.
7. Ellahi R, Hassan M, Zeeshan A. Aggregation effects on water base Al_2O_3-nanofluid over permeable wedge in mixed convection. Asia Pac J Chem Eng. 2016;11:179–86.
8. Dib A, Haiahem A, Bou-said B. Approximate analytical solution of squeezing unsteady nanofluid flow. Powder Technol. 2015;269:193–9.
9. Hayat T, Hussain Z, Alsaedi A, Mustafa M. Nanofluid flow through a porous space with convective conditions and heterogeneous–homogeneous reactions. J Taiwan Inst Chem Eng. 2016. https://doi.org/10.1016/j.jtice.2016.11.002.
10. Hayat T, Imtiaz M, Alsaedi A, Alzahrani F. Effects of homogeneous–heterogeneous reactions in flow of magnetite-Fe_3O_4 nanoparticles by a rotating disk. J Mol Liq. 2016;216:845–55.
11. Rashidi MM, Ganesh NV, Hakeem AKA, Ganga B. Buoyancy effect on MHD flow of nanofluid over a stretching sheet in the presence of thermal radiation. J Mol Liq. 2014;198:234–8.
12. Bhatti MM, Rashidi MM. Effects of thermo-diffusion and thermal radiation on Williamson nanofluid over a porous shrinking/stretching sheet. J Mol Liq. 2016;221:567–73.
13. Dogonchi AS, Chamkha Ali J, Seyyedi SM, Ganji DD. Radiative nanofluid flow and heat transfer between parallel disks with penetrable and stretchable walls considering Cattaneo–Christov heat flux model. Heat Transf Asian Res. 2018;47:735–53. https://doi.org/10.1002/htj.21339.
14. Dogonchi AS, Alizadeh M, Ganji DD. Investigation of MHD Go-water nanofluid flow and heat transfer in a porous channel in the presence of thermal radiation effect. Adv Powder Technol. 2017;28:1815–25.
15. Dogonchi AS, Divsalar K, Ganji DD. Flow and heat transfer of MHD nanofluid between parallel plates in the presence of thermal radiation. Comput Methods Appl Mech Eng. 2016;310:58–76.
16. Dogonchi AS, Ganji DD. Thermal radiation effect on the nanofluid buoyancy flow and heat transfer over a stretching sheet considering Brownian motion. J Mol Liq. 2016;223:521–7.
17. Dogonchi AS, Ganji DD. Effects of Cattaneo–Christov heat flux on buoyancy MHD nanofluid flow and heat transfer over a stretching sheet in the presence of Joule heating and thermal radiation impacts. Indian J Phys. 2018;92:757–66.
18. Alizadeh M, Dogonchi AS, Ganji DD. Micropolar nanofluid flow and heat transfer between penetrable walls in the presence of thermal radiation and magnetic field. Case Stud Therm Eng. 2018;12:319–32.
19. Dogonchi AS, Ganji DD. Study of nanofluid flow and heat transfer between non-parallel stretching walls considering Brownian motion. J Taiwan Inst Chem Eng. 2016;69:1–13.
20. Dogonchi AS, Ganji DD. Investigation of MHD nanofluid flow and heat transfer in a stretching/shrinking convergent/divergent channel considering thermal radiation. J Mol Liq. 2016;220:592–603.
21. RamReddy Ch, Murthy PVSN, Chamkha AJ, Rashad AM. Soret effect on mixed convection flow in a nanofluid under convective boundary condition. Int J Heat Mass Transf. 2013;64:384–92.
22. Selimefendigil F, Oztop HF. MHD mixed convection of nanofluid filled partially heated triangular enclosure with a rotating adiabatic cylinder. J Taiwan Inst Chem Eng. 2014;45:2150–62.
23. Selimefendigil F, Oztop HF. Numerical study of MHD mixed convection in a nanofluid filled lid driven square enclosure with a rotating cylinder. Int J Heat Mass Transf. 2014;78:741–54.
24. Selimefendigil F, Oztop HF, Chamkha AJ. MHD mixed convection and entropy generation of nanofluid filled lid driven cavity under the influence of inclined magnetic fields imposed to its upper and lower diagonal triangular domains. J Magn Magn Mater. 2016;406:266–81.
25. Selimefendigil F, Oztop HF. Mixed convection of nanofluids in a three dimensional cavity with two adiabatic inner rotating cylinders. Int J Heat Mass Transf. 2018;117:331–43.
26. Selimefendigil F, Öztop HF. Cooling of a partially elastic isothermal surface by nanofluids jet impingement. J Heat Transf. 2018;140(4):042205.
27. Selimefendigil F, Oztop HF. Numerical study and pod-based prediction of natural convection in a ferrofluids–filled triangular cavity with generalized neural network. Numer Heat Transf Part A Appl. 2016;67(10):1136–61.
28. Sheremet MA, Grosan T, Pop I. Natural convection and entropy generation in a square cavity with variable temperature side walls filled with a nanofluid: Buongiorno's mathematical model. Entropy. 2017;19:337. https://doi.org/10.3390/e19070337.
29. Ghalambaz M, Doostani A, Izadpanahi E, Chamkha AJ. Phase-change heat transfer in a cavity heated from below: the effect of utilizing single or hybrid nanoparticles as additives. J Taiwan Inst Chem Eng. 2017;72:104–15.
30. Alsabery A, Chamkha AJ, Hashim I. Heatline visualization of conjugate natural convection in a square cavity filled with nanofluid with sinusoidal temperature variations on both horizontal walls. Int J Heat Mass Transf. 2016;100:835–50.
31. Rashad AM, Rashidi MM, Lorenzini G, Ahmed SE, Aly AM. Magnetic field and internal heat generation effects on the free convection in a rectangular cavity filled with a porous medium saturated with Cu–water nanofluid. Int J Heat Mass Transf. 2017;104:878–89.
32. Sheremet MA, Revnic C, Pop I. Free convection in a porous wavy cavity filled with a nanofluid using Buongiorno's mathematical model with thermal dispersion effect. Appl Math Comput. 2017;299:1–15.
33. Bararnia H, Hooman K, Ganji DD. Natural convection in a nanofluid filled portion cavity; the Lattice-Boltzmann method. Numer Heat Transf Part A. 2011;59:487–502.
34. Abu-Nada E, Masoud Z, Hijazi A. Natural convection heat transfer enhancement in horizontal concentric annuli using nanofluids. Int Commun Heat Mass Transf. 2008;35:657–65.
35. Jou RY, Tzeng SC. Numerical research of nature convective heat transfer enhancement filled with nanofluids in rectangular enclosures. Int Commun Heat Mass Transf. 2006;33:727–36.
36. Dogonchi AS, Chamkha AJ, Ganji DD. A numerical investigation of magneto-hydrodynamic natural convection of Cu–water nanofluid in a wavy cavity using CVFEM. J Therm Anal Calorim. 2018. https://doi.org/10.1007/s10973-018-7339-z.
37. Selimefendigil F, Oztop HF, Abu-Hamdeh N. Natural convection and entropy generation in nanofluid filled entrapped trapezoidal cavities under the influence of magnetic field. Entropy. 2016;18(2):43.
38. Sheremet MA, Cimpean DS, Pop I. Free convection in a partially heated wavy porous cavity filled with a nanofluid under the effects of Brownian diffusion and thermophoresis. Appl Therm Eng. 2017;113:413–8.

39. Ben-Nakhi A, Chamkha AJ. Conjugate natural convection in a square enclosure with inclined thin fin of arbitrary length. Int J Therm Sci. 2007;46:467–78.
40. Chamkha AJ. Double-diffusive convection in a porous enclosure with cooperating temperature and concentration gradients and heat generation or absorption effects. Numer Heat Transf A. 2002;41:65–87.
41. Ben-Nakhi A, Chamkha AJ. Effect of length and inclination of a thin fin on natural convection in a square enclosure. Numer Heat Transf A. 2006;50:381–99.
42. Chamkha AJ, Grosan T, Pop I. Fully developed free convection of a micropolar fluid in a vertical channel. Int Commun Heat Mass Transf. 2002;29:1119–27.
43. Selimefendigil F, Oztop HF. Role of magnetic field and surface corrugation on natural convection in a nanofluid filled 3D trapezoidal cavity. Int Commun Heat Mass Transf. 2018;45:182–96.
44. Dogonchi AS, Sheremet MA, Ganji DD, Pop I. Free convection of copper–water nanofluid in a porous gap between hot rectangular cylinder and cold circular cylinder under the effect of inclined magnetic field. J Therm Anal Calorim. 2018. https://doi.org/10.1007/s10973-018-7396-3.
45. Khanafer K, Vafai K, Lightstone M. Buoyancy-driven heat transfer enhancement in a two dimensional enclosure utilizing nanofluids. Int J Heat Mass Transf. 2003;46:3639–53.
46. De Vahl Davis G. Natural convection of air in a square cavity, a benchmark numerical solution. Int J Numer Methods Fluids. 1962;3:249–64.